Supplementary Information for

Structure of histone mRNA stem-loop, human stem-loop binding protein and 3'hExo ternary complex

Dazhi Tan,[1] William F. Marzluff,[2,3] Zbigniew Dominski,[2,3] Liang Tong[1]

[1]Department of Biological Sciences
Columbia University
New York, NY 10027, USA

[2]Department of Biochemistry and Biophysics
[3]Program in Molecular Biology and Biotechnology
University of North Carolina at Chapel Hill
Chapel Hill, NC 27599, USA

Correspondence information for Liang Tong

Phone: (212) 854-5203, FAX: (212) 865-8246

E-mail: ltong@columbia.edu

Materials and Methods

Protein expression and purification. Residues 55-349 of human 3'hExo were sub-cloned into the pET-24d vector (Novagen) and the recombinant protein carried a C-terminal 6×His-tag. Residues 125-223 of human SLBP were sub-cloned into the pET-28a vector (Novagen), which introduced an N-terminal 6×His-tag. BL21 (DE3) Star cells transformed with either plasmid were induced with 0.4 mM IPTG and allowed to grow at either 16 °C (for 3'hExo) or 24 °C (for SLBP) for 18 h. The soluble proteins were purified through nickel-agarose affinity (Qiagen) and cation-exchange (SP Sepharose Fast Flow; GE Healthcare) chromatography. Particularly for the purification of SLBP, 0.2% Triton X-100 was included in the elution buffer for nickel-agarose affinity chromatography to enhance its solubility. The purified proteins were concentrated and stored at –80 ºC in a buffer containing 20 mM HEPES (pH 7.0), 500 mM NaCl, 5 mM DTT and 5% (v/v) glycerol. The His-tag was not removed for crystallization.

The selenomethionyl human 3'hExo (55-349) protein was produced in *E. coli* B834 (DE3) cells and the bacteria were grown in defined LeMaster medium supplemented with selenomethione (*1*). The purification procedure is the same as for the native protein.

The 26 nt stem-loop RNA (5'-CCAAAGGCUCUUUUCAGAGCCACCCA-3') was purchased from Integrated DNA Technologies (IDT), annealed by heating to 90 °C for 2 min followed by cooling in ice water for 5 min. To form the SLBP-3'hExo-SL ternary complex, the proteins and the RNA were mixed with 1:1:1 stoichiometry and incubated on ice for 30 min prior to gel-filtration chromatography (Sephacryl S-300; GE Healthcare). Fractions corresponding to the ternary complex were collected and concentrated to 5 mg/mL in a buffer containing 20 mM HEPES (pH 7.0), 300 mM NaCl, 5mM DTT and 5% (v/v) glycerol.

Protein crystallization. Divalent metal ions were excluded from the solutions to prevent SL hydrolysis by 3′hExo. Small crystals of the ternary complex were obtained with the sitting-drop vapor-diffusion method at 20 °C. The reservoir contains 8% (w/v) Tacsimate (pH 6.0) (Hampton Research) and 18% (w/v) PEG3350 (Sigma-Aldrich). The quality of the crystals was significantly improved through macroseeding and the addition of 10 mM hexaaminecobalt(III) chloride (Hampton Research) as an additive in the crystallization drop. Two related crystal forms were observed, both belonging to space group $P2_12_12_1$, with unit cell parameters of a=81.8 Å, b=90.8 Å, c=128.6 Å or a=75.6 Å, b=90.6 Å, c=128.1 Å. There is one SLBP-3'hExo-SL ternary complex and one 3'hExo-SL binary complex in the asymmetric unit. The structure in the first crystal form is described here, and that in the second crystal form is generally similar.

Data collection and structure determination. A single-wavelength anomalous diffraction (SAD) data set to 2.6 Å resolution was collected on an ADSC charge-coupled device at the X29A beamline of National Synchrotron Light Source (NSLS). The diffraction images were processed and scaled with the HKL package (*2*). The resolution limit was decided based on R_{merge}, I/σI and completeness considerations (Table S1).

The nuclease domain of 3'hExo was located in the crystal with the program COMO (*3*), using the previously reported structure of this domain as the search model (*4*). The Se sites (18 total for the two 3'hExo molecules) were located in an anomalous difference electron density map, using phases calculated based on the nuclease domain. Reflection phases were calculated and improved based on the SAD data with Solve/Resolve (*5*),

which also traced a majority of the residues. The atomic model was completed with manual building with the program Coot (*6*). The structure refinement was carried out with the program CNS (*7*), and the anomalous scattering of Se atoms was included in the refinement. The statistics on the crystallographic data and structure refinement are summarized in Table S1.

Mutagenesis. The SLBP and 3'hExo mutants were designed based on the structural information, generated with the QuikChange kit (Stratagene), and verified through sequencing. The mutant proteins were purified with the same protocol as the wild-type proteins. They had the same gel filtration profiles as the wild-type SLBP or 3′hExo, suggesting that the mutations did not cause global disruption of the structures.

Electrophoretic mobility shift assays (EMSA) for the binary complexes. The stem-loop RNA with a 6-FAM fluorescence label at the 5'-end was purchased from IDT. Prior to the assays, the RNA was heated at 94 °C for 5 min and then slow-cooled to room temperature. 20 pmol of the RNA was mixed with 20 pmol of 3'hExo and/or 30 pmol of SLBP RBD in a buffer containing 20 mM HEPES (pH 7.0), 50 mM NaCl, and 1 mM EDTA, in a total volume of 20 μL and incubated on ice for 30 min. The samples were loaded to a 1.5% native agarose gel for the binary complex and 0.5% agarose gel for the ternary complex. The electrophoresis was performed in 1× TAE buffer (pH 8.0) at 4 °C, and then the RNA bands were visualized on a UV illuminator.

References:

1. W. A. Hendrickson, J. R. Horton, D. M. LeMaster, *EMBO J.* **9**, 1665 (1990).
2. Z. Otwinowski, W. Minor, *Method Enzymol.* **276**, 307 (1997).
3. G. Jogl, X. Tao, Y. Xu, L. Tong, *Acta Cryst.* **D57**, 1127 (2001).
4. Y. Cheng, D. J. Patel, *J. Mol. Biol.* **343**, 305 (2004).
5. T. C. Terwilliger, *Meth. Enzymol.* **374**, 22 (2003).
6. P. Emsley, K. D. Cowtan, *Acta Cryst.* **D60**, 2126 (2004).
7. A. T. Brunger *et al.*, *Acta Cryst.* **D54**, 905 (1998).
8. W. F. Marzluff, *Curr. Opin. Cell Biol.* **17**, 274 (2005).
9. Z. Dominski, W. F. Marzluff, *Gene* **396**, 373 (2007).
10. W. F. Marzluff, E. J. Wagner, R. J. Duronio, *Nat. Rev. Genet.* **9**, 843 (2008).
11. R. Thapar, W. F. Marzluff, M. R. Redinbo, *Biochem.* **43**, 9401 (2004).
12. Z. Dominski, J. A. Erkmann, J. A. Greenland, W. F. Marzluff, *Mol. Cell. Biol.* **21**, 2008 (2001).
13. D. C. Avgousti, S. Palani, Y. Sherman, A. Grishok, *EMBO J.* **31**, 3821 (2012).
14. M. D. Lopez, T. Samuelsson, *RNA* **14**, 1 (2008).
15. E. S. DeJong, W. F. Marzluff, E. P. Nikonowicz, *RNA* **8**, 83 (2002).
16. K. Zanier *et al.*, *RNA* **8**, 29 (2002).
17. K. P. Hoefig *et al.*, *Nature Struct. Mol. Biol.*, (2012).
18. X. J. Lu, W. K. Olson, *Nucl. Acid Res.* **31**, 5108 (2003).
19. F. Martin, F. Michel, D. Zenklusen, B. Muller, D. Schumperli, *Nucl. Acid Res.* **28**, 1594 (2000).
20. C. H. Borchers *et al.*, *Proc. Natl. Acad. Sci. USA* **103**, 3094 (2006).
21. F. Michel, D. Schumperli, B. Muller, *RNA* **6**, 1539 (2000).
22. S. Jaeger, G. Eriani, F. Martin, *FEBS Lett.* **556**, 265 (2004).
23. X.-C. Yang, M. Purdy, W. F. Marzluff, Z. Dominski, *J. Biol. Chem.* **281**, 30447 (2006).

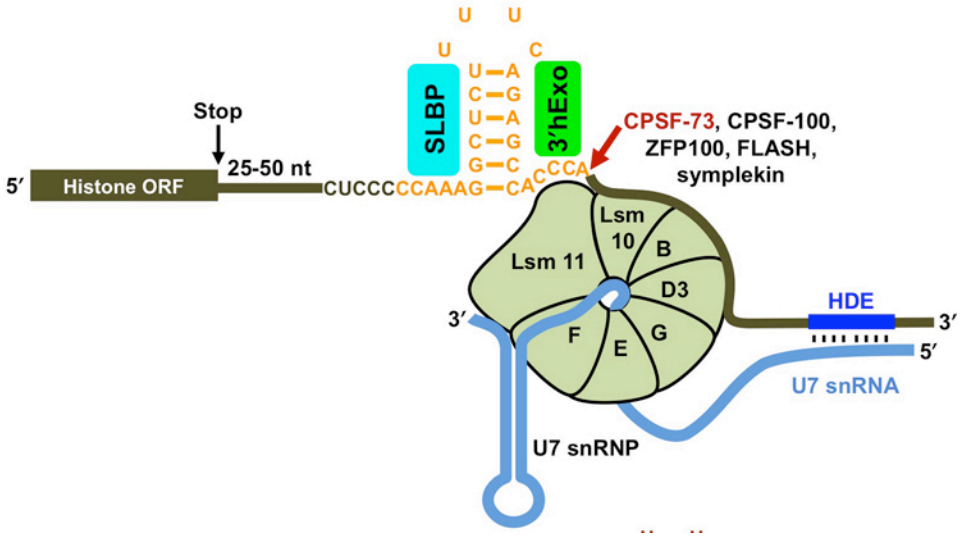

Fig. S1. Factors involved in histone pre-mRNA 3'-end processing (*8-10*). The 3'-end contains a stem-loop (SL) within 50 nt of the STOP codon. The 26 nt SL RNA used in the current study is shown (orange). The cleavage occurs 4-5 nt downstream of the stem, which is followed by the histone downstream element (HDE, blue). SLBP (cyan) interacts with the 5' side of the stem-loop, while 3'hExo (green) interacts with the 3' side. The HDE base pairs with the 5'-end of the U7 snRNA (light blue). The two unique protein components of the U7 snRNP ring (light green), Lsm10 and Lsm11, mediate interactions in this 3'-end processing complex. Additional protein factors, such as ZFP100, CPSF-73, CPSF-100, symplekin, and FLASH are also shown. CPSF-73 (red) is the endonuclease that cleaves the histone pre-mRNA.

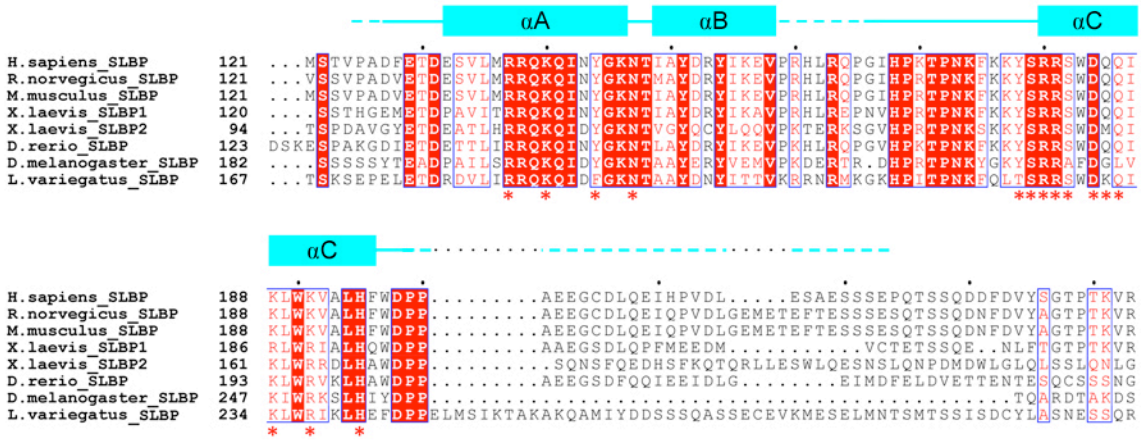

Fig. S2. Sequence alignment of SLBP from various organisms. The RBD is shown in cyan for the secondary structures. Dashed lines indicate residues that are disordered in the crystal, and dots indicate gaps in the alignment. Residues in contact with stem-loop RNA are marked with the red asterisks. Residues N-terminal to the RBD are not shown.

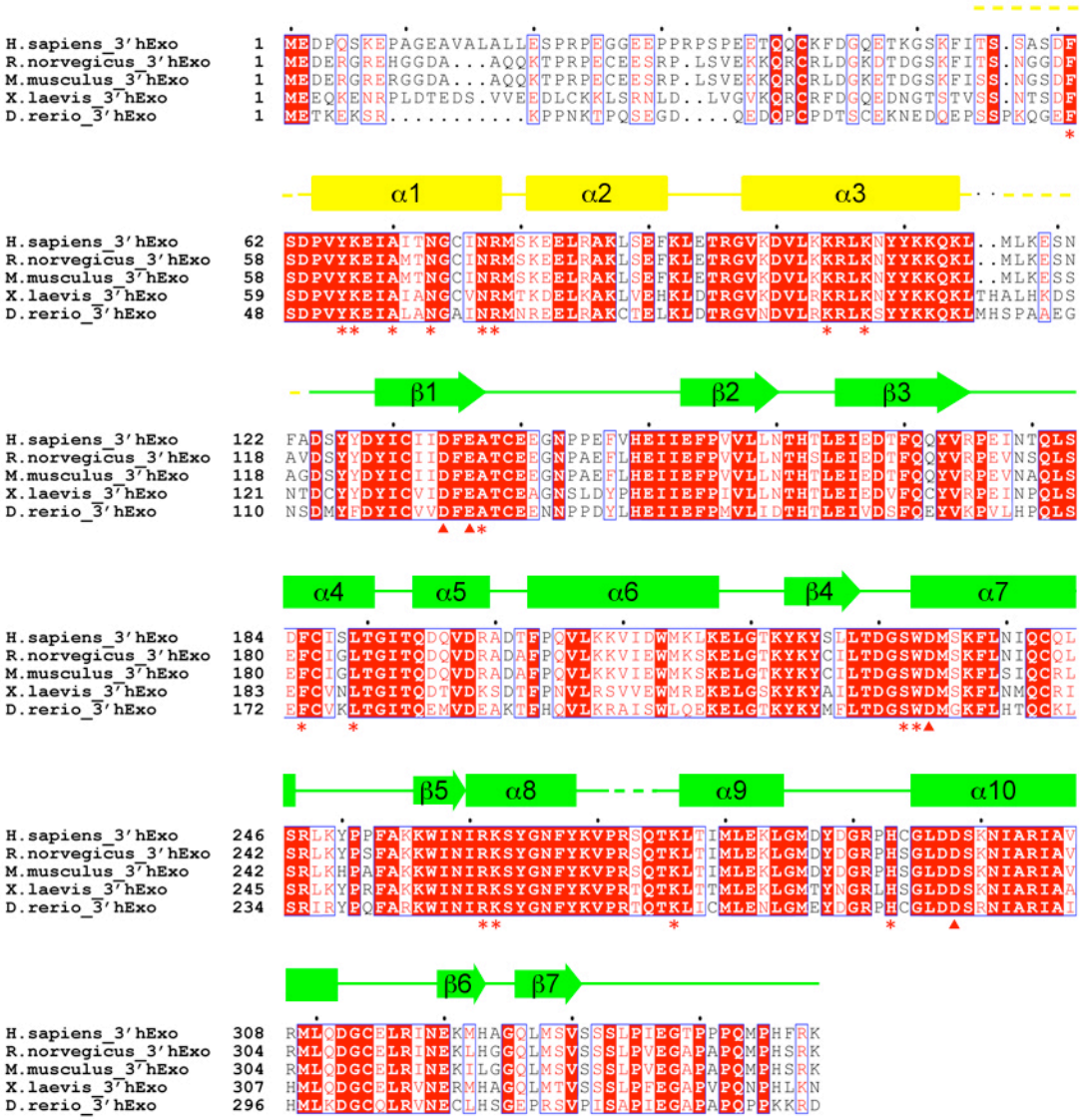

Fig. S3. Sequence alignment of 3'hExo from various organisms. The SAP domain (yellow for secondary structure elements) contains helices α1-α3, and the remaining C-terminal residues are in the nuclease domain (green). The four acidic residues that coordinate the metal ions are indicated with the red triangles. Residues in contact with stem-loop RNA are marked with the red asterisks.

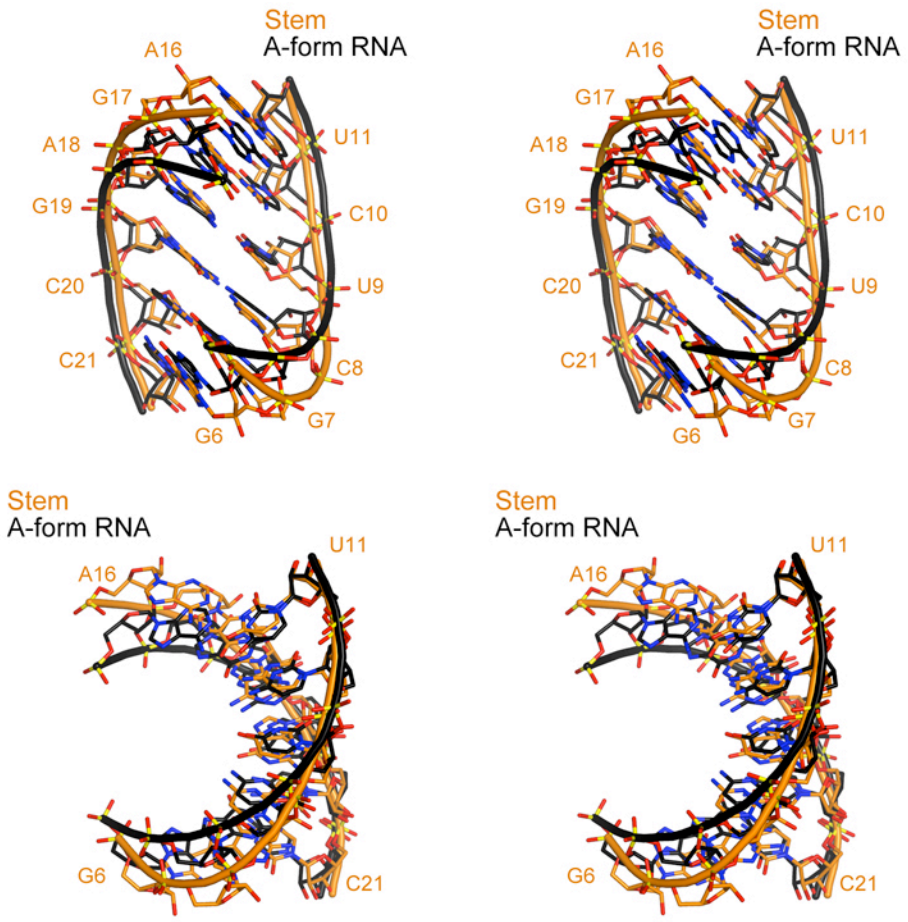

Fig. S4. Two different views in stereo of the overlay of the structure of the stem (orange) with a classical A-form RNA (black). The stem is more flattened compared to the A-form RNA.

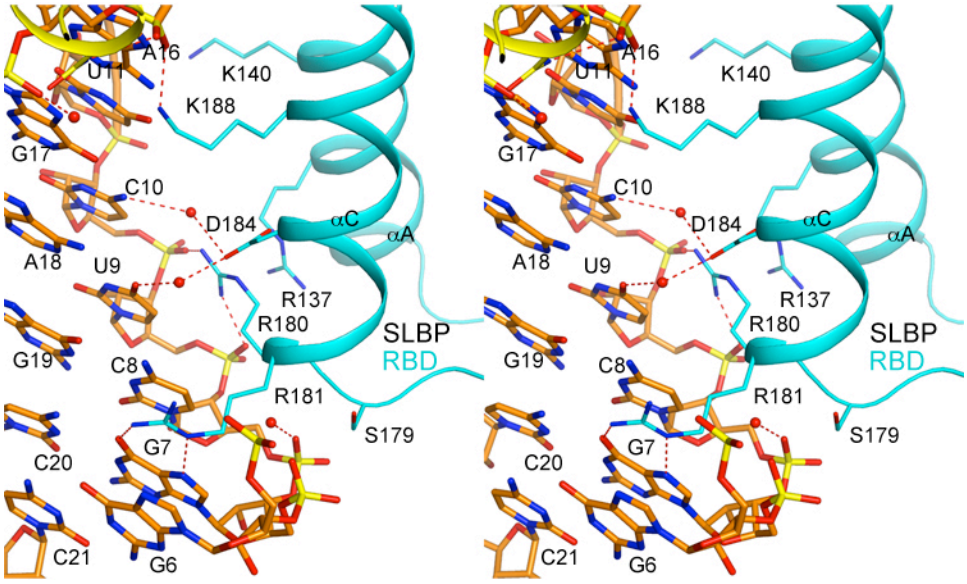

Fig. S5. Interactions between SLBP RBD (cyan) and the stem of the SL RNA (orange). Water molecules are shown as red spheres. Additional observations on the interactions:

(1) The side chain of Asp184 (αC) is hydrogen-bonded to the bases of U9 and C10 through two waters. The side chain of Lys191 (αC) is hydrogen-bonded to the 2' hydroxyl and the base of U14.

(2) The 5' phosphate group of the third nucleotide in the stem (C8) is hydrogen-bonded to the main-chain amide of residue 180 at the N-terminus of helix αC, and therefore this phosphate group (as well as that of G7) also has favorable interactions with the dipole of this helix. Ionic interactions between positively-charged side chains and the phosphate groups of the RNA include Arg137 (αA) and Arg180 (αC) with U9 and C10 of the stem, Lys140 (αA) with U12 of the loop, Lys188 (αC) with A16.

(3) Nucleotides 1-2 do not interact with SLBP RBD. Nucleotide 1 interacts with the SAP domain of a neighboring 3'hExo molecule in the crystal, and this crystal packing contact may have partly stabilized the conformation of the 5'-end of the SL.

(4) Residues 159-164 in the loop between αB and αC are disordered and not included in the current atomic model (Fig. 1C). These residues are not expected to participate in RNA binding.

(5) *Drosophila* SLBP was reported to be devoid of stable three-dimensional fold on its own, and binding of RNA (together with phosphorylation of a C-terminal segment outside of the RBD) is important for its proper folding (*11*). In comparison, the RBD of human SLBP appears to be relatively stable in our experiments.

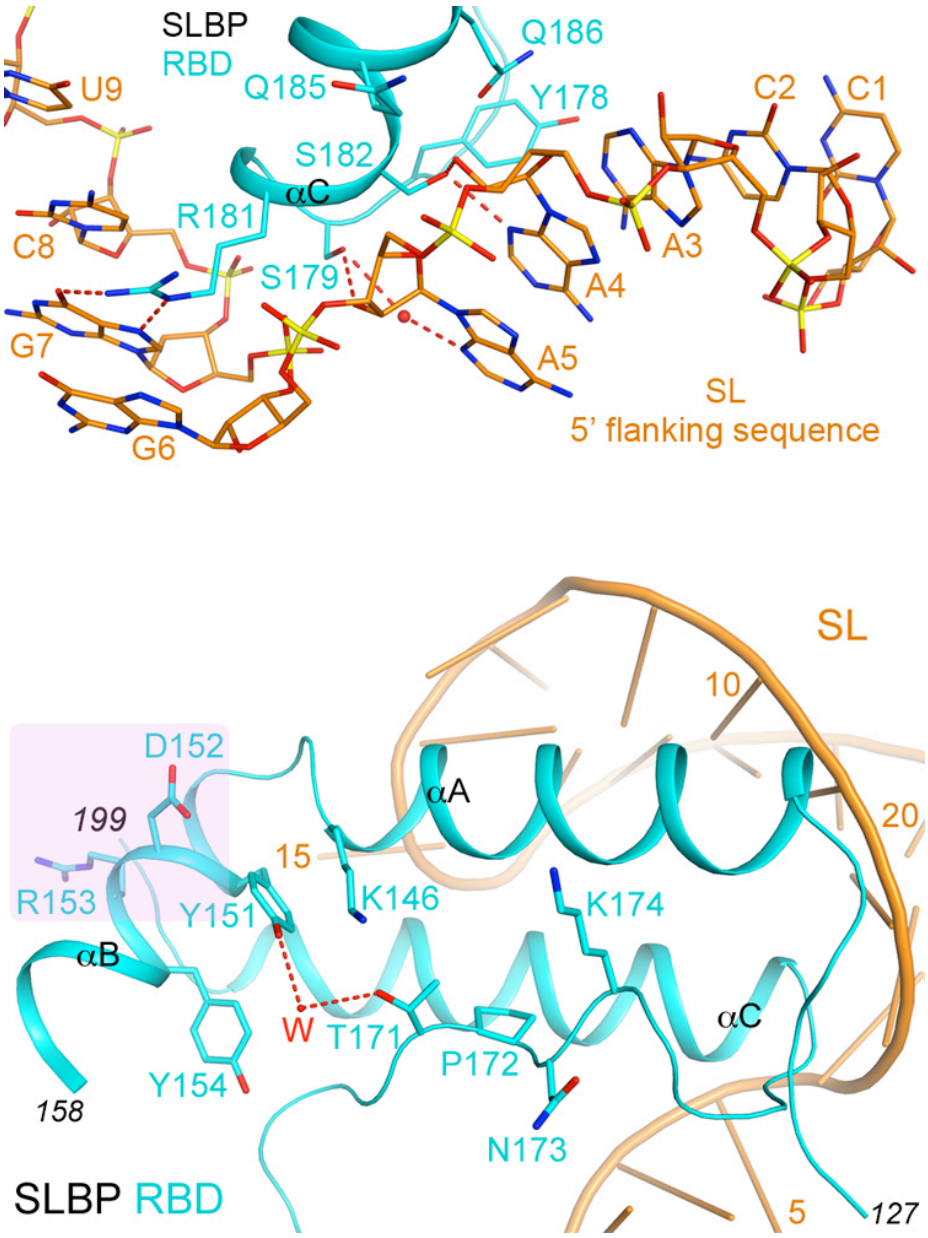

Fig. S6. (***Top***) Interactions between the 5' flanking sequence (CCAAA) of SL with SLBP RBD helix αC and the loop preceding it. (***Bottom***) Conformation of residues 171-TPNK-174 in the ternary complex. A water molecule (labeled W) likely occupies the position of one of the oxygen atoms on the phosphate of pT171, and is hydrogen-bonded to the side chain of Tyr151. The loop containing these residues is on the opposite face of SLBP RBD from the SL RNA. The pink highlight indicates a surface region formed by residues Asp152, Arg153 and the 20 residues following 199, which is important for processing but not for SL binding (*12*).

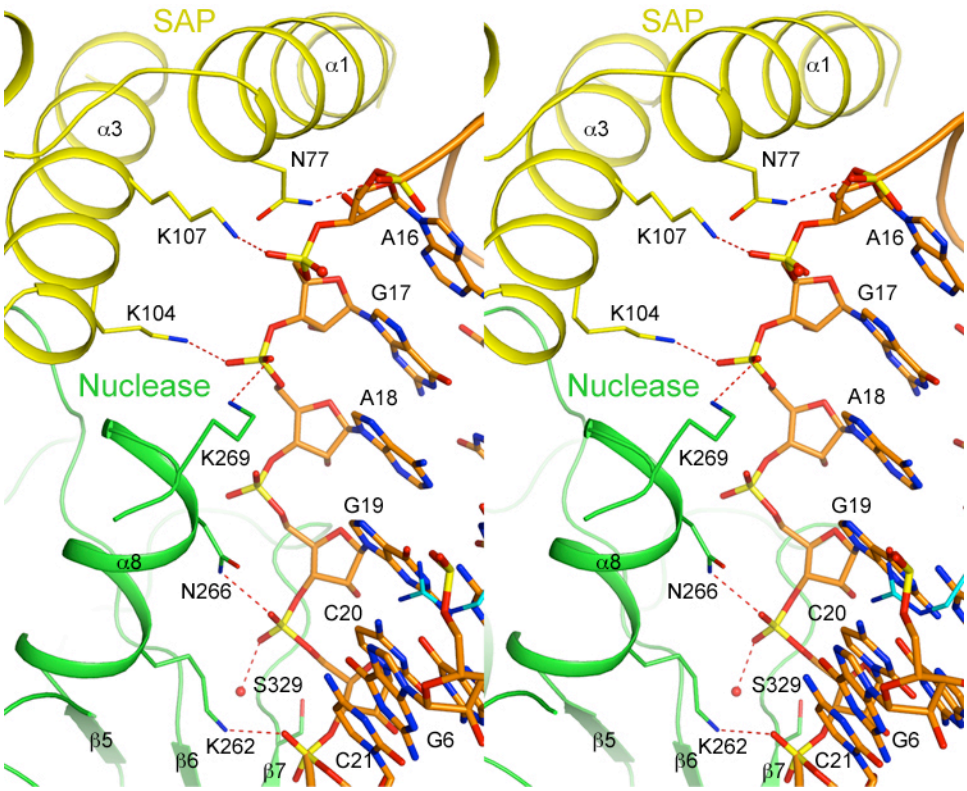

Fig. S7. Interactions between the SAP (yellow) and nuclease (green) domains of 3'hExo and the stem of the SL RNA (orange). Additional observations on the interactions:

(1) The side chain of Asn73 (α1) is hydrogen-bonded to the hydroxyl on the ribose of A16, and that of Asn77 is hydrogen-bonded to the phosphate group of this nucleotide. The side chain of Lys67 has ionic interactions with the phosphate group of U14 (Fig. 2B). The main-chain carbonyl oxygen atom of Ala70 (α1) is also hydrogen-bonded to the 2' hydroxyl group of C15.

(2) In a related crystal, the side chain of Phe61 (in a loop prior to α1) is also positioned next to the U13 base, although this side chain is involved in crystal packing as well. In the current crystal, residue 61 is disordered.

(3) From helix α3, the side chains of Lys104 and Lys107 have ionic interactions with the phosphate groups of nucleotides 17 and 18 in the stem.

(4) Helices α1 and α3 in the SAP domain and helix α8 in the nuclease domain have very different orientations relative to the stem.

(5) Residues 117-123 in the linker between the SAP and nuclease domains are disordered and not included in the current model.

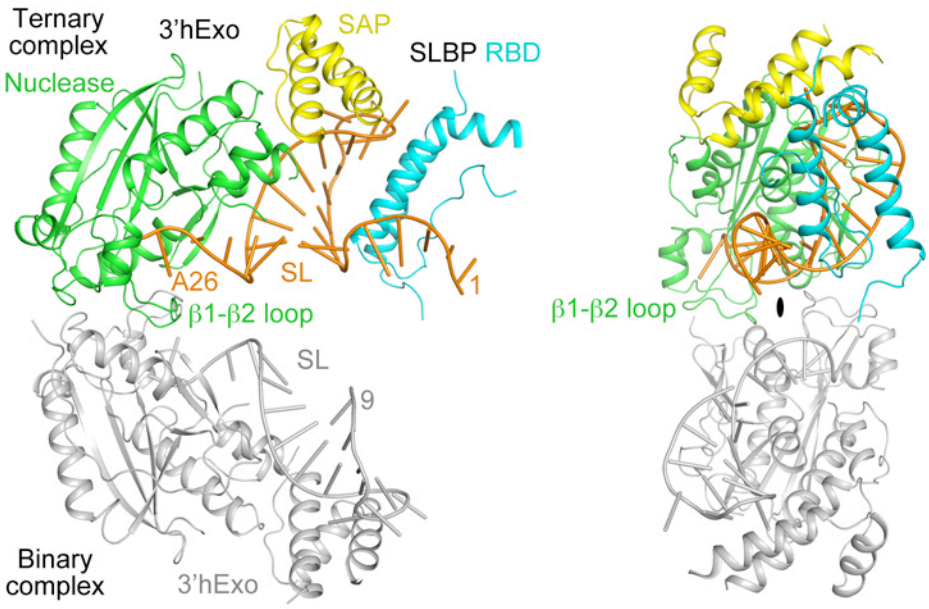

Fig. S8. (***Left***) The ternary (in color) and binary (in gray) complexes are related by a non-crystallographic two-fold axis (along the horizontal direction) in the crystal. The β1-β2 loop of the nuclease domain is located in the dimer interface. This loop contains residue Asn143, which forms one wall of the binding site for A26 (Fig. 3B). (***Right***) The two complexes viewed down the two-fold axis (black oval).

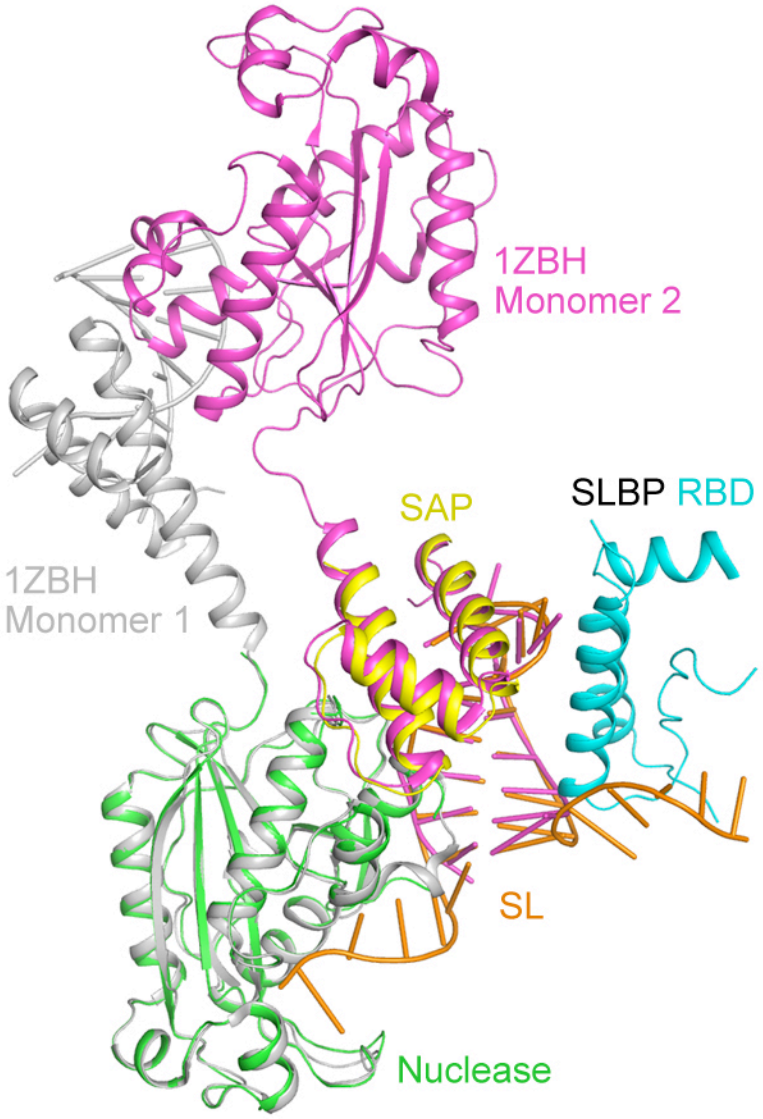

Fig. S9. Overlay of the structures of the SLBP-3'hExo-SL ternary complex with that of a domain-swapped dimer of 3'hExo-RNA complex (PDB entry 1ZBH, in gray and magenta for the two monomers). The RNA in the 1ZBH structure contains only the stem and the loop, with no flanking sequence at either the 5' or 3' end, and therefore does not show RNA binding in the active site. The SAP domain from the second monomer (magenta) is located close to the SAP domain in the ternary complex (yellow). The 1ZBH structure also contains two additional nuclease domains (not shown), and their SAP domains are disordered. Arg272 caps the 3'-end of the stem, being π-stacked with the last base in that structure. Such a conformation is not possible in the current structure as the last base of the stem is π-stacked with A22. Residues 271-273 are disordered in the current structure.

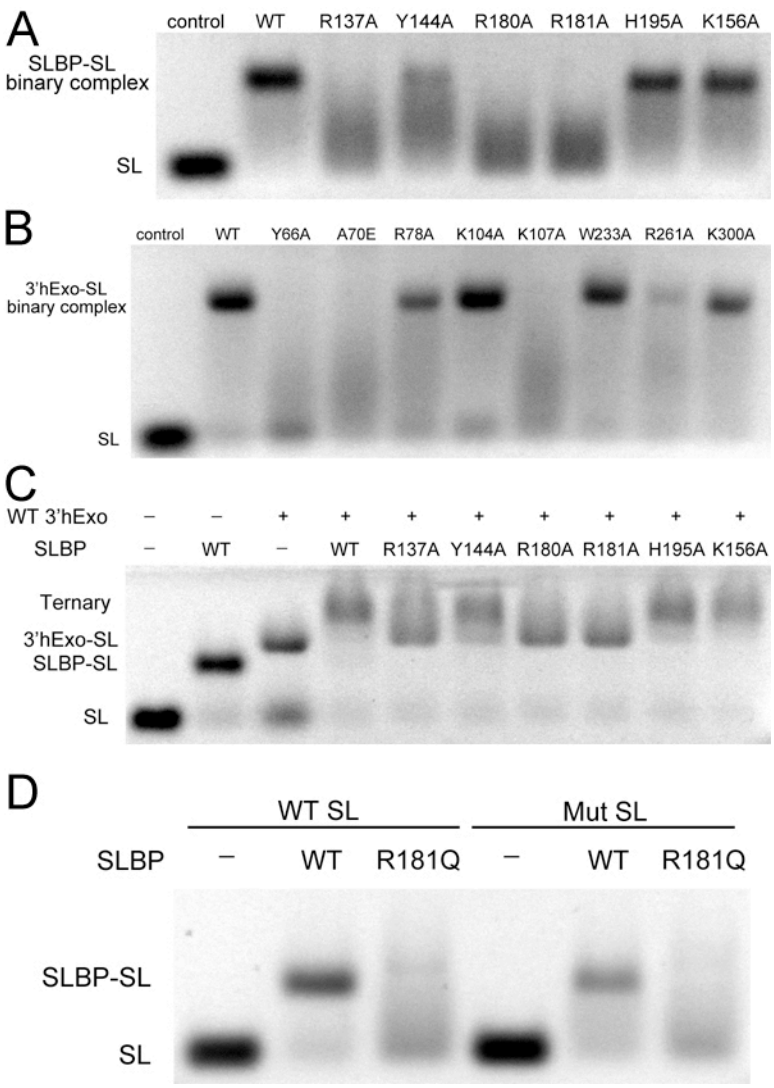

Fig. S10. Electrophoretic mobility shift assays on binary and ternary complexes. **(A)**. Effect of mutations in the SL-SLBP RBD interface on the formation of the binary complex. The K156A mutation is a control. **(B)**. Effect of mutations in the SL-3′hExo interface on the formation of the binary complex. The K300A mutation is a control. Our nuclease assays also confirmed that the W233A mutant was still catalytically active. **(C)**. Effect of mutations in the SL-SLBP interface on the formation of the ternary complex. The SLBP Y144A mutation appears to disturb binary complex formation, but the mutant can be incorporated into the ternary complex, an evidence for the cooperative effect of binding between SLBP and 3′hExo. **(D)**. The R181Q mutant does not have stronger binding to a stem-loop mutant with an A-U base pair at the second position of the stem (Mut SL) compared to the wild-type SL. Our modeling studies with this mutant suggest that the Gln side chain can probably form a good hydrogen bond only with the N7 atom, and therefore could not readily distinguish between A and G and has weaker interactions overall with the SL. On the other hand, wild-type SLBP RBD showed appreciable binding to this SL mutant.

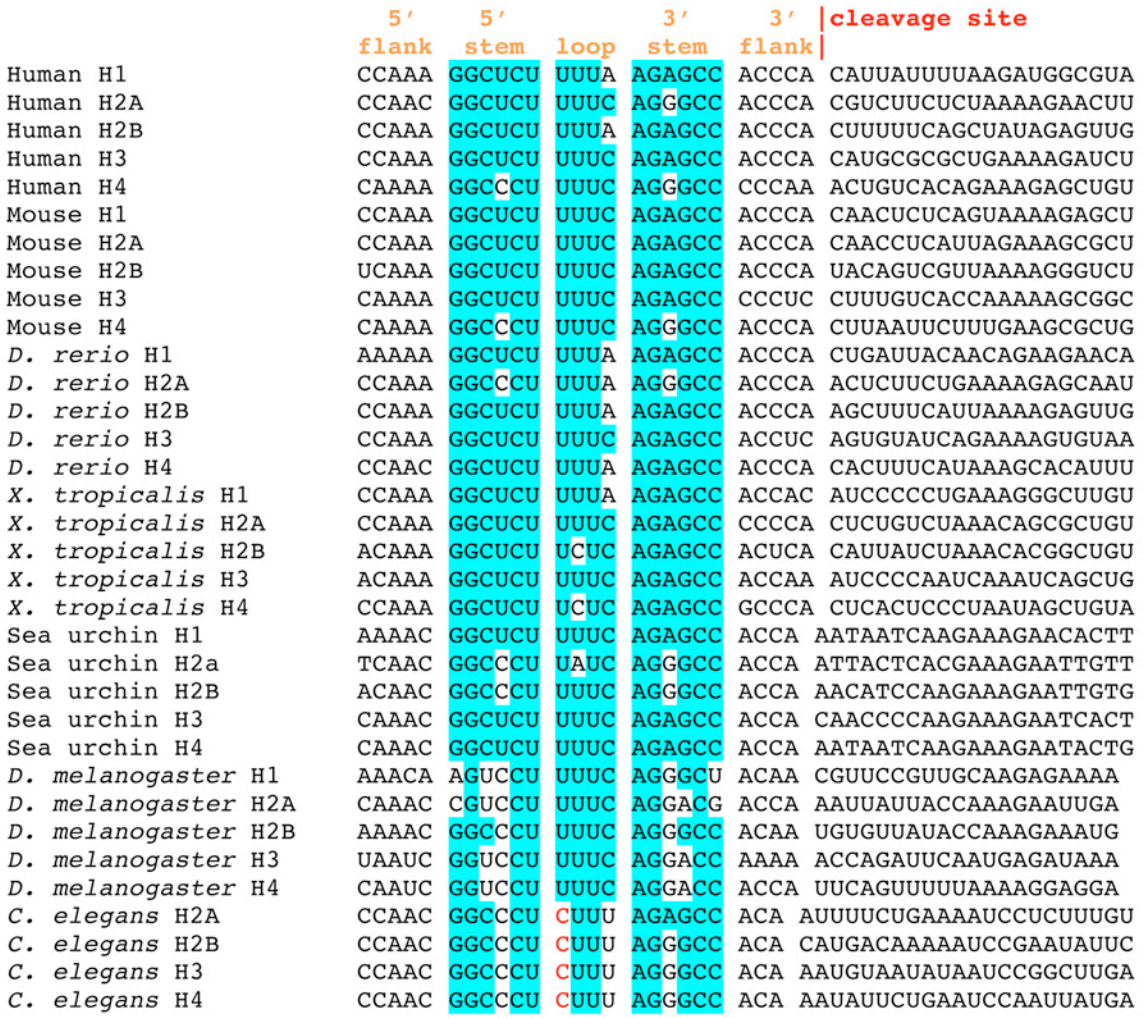

Fig. S11. Alignment of histone pre-mRNA sequences near the stem-loop. One sequence is shown for each type of histones in each organism. The consensus sequence in the stem-loop is highlighted in cyan. *C. elegans* histone mRNAs have a C at the first position of the loop (in red), distinct from the other histone mRNAs. Histone pre-mRNA processing in *C. elegans* is mediated by SLBP and an RNAi pathway, as this organism lacks U7 snRNP, and the cleavage site indicates the end of mature mRNAs (*13*). The sequences (except those for sea urchin) are obtained from (*14*). Sea urchin: *Psammechinus milaris.*

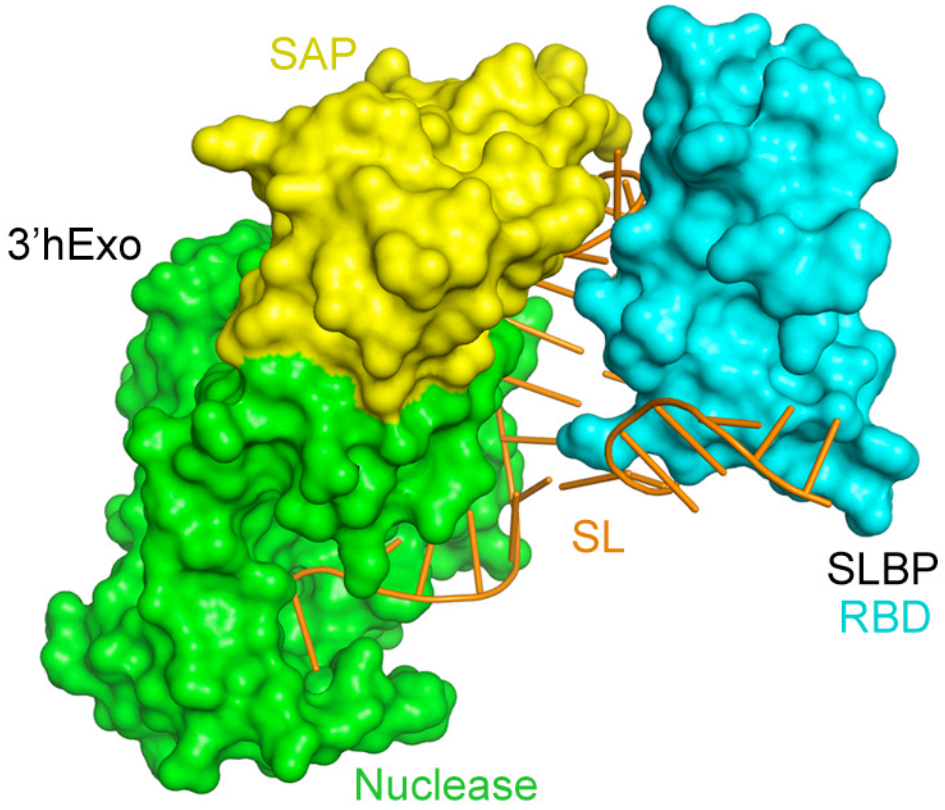

Fig. S12. No contacts between SLBP RBD and 3'hExo in the ternary complex. The proteins are shown as molecular surfaces, colored by the domains. There is a clear gap between the two proteins, bridged by the SL RNA.

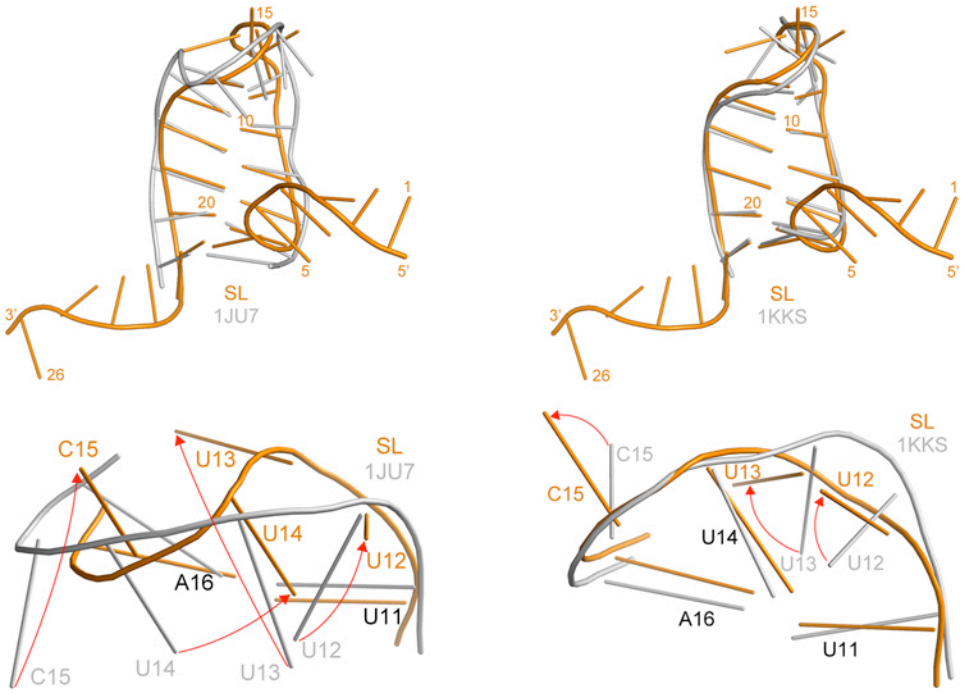

Fig. S13. (***Left***) Overlay of the SL structure in the ternary complex (orange) with that of a 26-nt SL RNA alone in solution (gray) (PDB entry 1JU7) (*15*). The 5' and 3' flanking sequences are highly flexible in solution and are not shown. Large conformational differences in the stem and especially the loop are apparent. A closeup of the loop region is shown in the lower left. The positions of the bases in the loop are strikingly different in the two structures (indicated with the red arrows). (***Right***) Overlay of the SL structure in the ternary complex (orange) with that of an RNA with an extended stem and loop in solution (gray) (PDB entry 1KKS) (*16*). The stem was extended with four nucleotides at each end (not shown for clarity), capable of forming two GC base pairs. A closeup of the loop region is shown in the lower right. While the backbone of the loop assumes a similar conformation as in the ternary complex, the bases in the loop have different conformations. Especially, the base of U12 is π-stacked with that of U14 in solution, while it is flipped out in the complex.

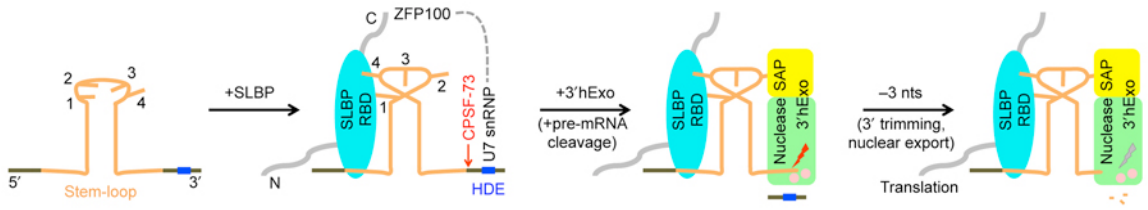

Fig. S14. A model relating our structural observations to the functions of SLBP and 3′hExo in histone mRNA maturation and function. The bases in the loop are indicated and labeled. Cleavage of the histone pre-mRNA occurs prior to the binding of 3′hExo to the new 3′-end. After trimming, the mRNA can no longer reach the active site of 3′hExo in the ternary complex. Upon export to the cytoplasm, the N-terminal segment of SLBP promotes translation of the histone mRNA. The eviction of SLBP from this ternary complex at the end of the S phase probably precedes complete degradation of the histone mRNA. Our structure of the binary complex suggests that 3′hExo might initiate degradation of the stem-loop in the absence of SLBP (*17*), by promoting dissociation of the last 3 bps of the stem.

Table S1

Summary of crystallographic information

Resolution range (Å) [1]	40-2.6 (2.69–2.6)
Number of observations	248,965
Wavelength	0.9793 Å
Redundancy	4.5 (4.0)
R_{merge} (%)	8.5 (43.9)
I/σI	15.1 (3.1)
Number of reflections[2]	53,219
Completeness (%)	94 (77)
R factor (%)	19.9 (31.7)
Free *R* factor (%)	24.9 (36.4)
rms deviation in bond lengths (Å)	0.008
rms deviation in bond angles (°)	1.3

1. The numbers in parentheses are for the highest resolution shell.

2. The Friedel pairs were kept as separate reflections during the refinement.

Table S2.

Helical parameters for the stem

Base pair step	X-disp (Å)	Incline (°)	Rise (Å)	Twist (°)
1-2	-3.2	9.6	3.2	38.7
2-3	-5.0	1.2	3.0	27.6
3-4	-7.2	11.9	2.8	25.8
4-5	-5.3	1.1	3.1	27.2
5-6	-5.1	2.5	3.1	27.4
Average	-5.4	5.3	3.0	29.4
Classical A-form RNA	-4.0	15.3	2.8	33.0

Helical parameters were determined using the program 3DNA (*18*).

Table S3.

Structural interpretation of observations on SLBP and 3'hExo mutants reported earlier

Mutation	Observations	Structural interpretation
Yeast three-hybrid assays on mutations in the **SLBP** (*19*). Observations are maximum 3-AT concentration allowed for growth. Wild-type SLBP allows growth at >225 mM 3-AT.		
R137A/R138A	No growth at 2.5 mM 3-AT	R137 interacts with the SL RNA, R138 is important for maintaining the structural integrity of the RBD.
T171A	200 mM 3-AT	T171 is phosphorylated, which enhances binding by 7-fold (*20*).
T171I	50 mM 3-AT	See above
E157K	100 mM 3-AT	E157 is in helix αB, not interacting with SL and on the surface of the RBD.
R181Q	12 mM 3-AT	R181 recognizes the guanine base of the second base pair of the stem.
R181C	15 mM 3-AT	See above
D184N	2 mM 3-AT	D184 interacts with the SL through two waters, it also ion pairs with Arg180, which interacts with SL.
Electrophoretic mobility shift assays (EMSA) on mutations in the **SLBP** (*21*).		
144-YGKNT-148 to RAKEK (present in *C. elegans* SLBP)	Wild-type RBD has K_d of 4 nM for mouse and *C. elegans* SL. Mutant RBD has K_d of 5 nM for the *C. elegans* SL, but binds poorly to mouse SL.	Mouse SL has a U at the first position of the loop, while *C. elegans* SL has a C at this position. Y144 is π-stacked with this base. The change to R, together with the other changes, affect the recognition of this base.
175-FKKY-178 to LINF	Makes human RBD specific for human SL, and it binds weakly to *C. elegans* SL.	Y178 is located near the 5' flanking sequence of the SL.

Electrophoretic mobility shift assays (EMSA) on mutations in the **SLBP** (*12*). Observations are binding relative to wild-type (%).		
R137A/R138A	0	R137 interacts with the SL RNA, R138 is important for maintaining the structural integrity of the RBD.
Q139A/K140A/Q141A	0	K140 interacts with the SL. It may also be important for stabilizing the conformation of Y144.
K146R	100	K146 may interact with the phosphate on T171. It is not involved in SL binding (Fig. S6).
K146A	5	K146 may interact with the phosphate on T171. It is not involved in SL binding.
Y151F	5-10	Y151 may interact with the phosphate on T171. It is not involved in SL binding.
Y154F	50	Y154 is not involved in SL binding.
Y151F/Y154F	5-10	See above
Y151S/Y154S	0	See above
Y151T/Y154T	0	See above
H168F	5-10	H168 is not involved in SL binding.
W183I/W190I	0	Both residues are in the hydrophobic core of the RBD.
Yeast three-hybrid assays on mutations in the **SLBP** (*22*). Observations are maximum 3-AT concentration allowed for growth. Wild-type SLBP allows growth at >225 mM 3-AT.		
G145R	7.5 mM 3-AT	G145 does not interact with SL. No space for the large Arg side chain in the structure
G145T	>100 mM 3-AT	Thr side chain can be accommodated.
P172S	No growth	P172 important for T171 phosphorylation.
P172L	5 mM 3-AT	See above.
R181H	12.5 mM 3-AT	R181 recognizes the guanine base of the second base pair of the stem.
D184N	2.5 mM 3-AT	D184 interacts with the SL through two waters, it also ion pairs with Arg180, which interacts with SL.

Electrophoretic mobility shift assays (EMSA) on mutations in **3'hExo** (*23*). Observations are binding relative to wild-type (%).		
Δ76-110	0	Residues 76-110 are part of the SAP domain (excluding helix α1).
K92A	100	K92 does not interact with SL and does not have a structural role.
K99A	100	K99 does not interact with SL and does not have a structural role.
K104A	100	K104 interacts with the phosphate of A18 of SL.
K92A/K104A	100	See above
R105A	0	R105 does not interact with SL. It is important for structural integrity.
Y109A/Y110A	100	Neither residue interacts with SL.
K111A/K112A	0	K111 is hydrogen-bonded to the base of U13.

Table S4.

The effects of SLBP and 3'hExo mutants produced for this study on complex formation

Mutation	Structural role(s)	Effect on complex (Fig. S9)[1]
SLBP		
R137A	Interacts with the phosphates of U9 and C10 of the stem (Fig. S4)	Destabilized SL-SLBP complex. Destabilized ternary complex. Probably no effect on SL-3'hExo complex.
Y144A	π-stacking with the first (U12) and third (U14) bases of the loop (Fig. 2B)	Destabilized SL-SLBP complex. No apparent effect on ternary complex.
R180A	Interacts with the phosphates of U9 and C10 of the stem (Fig. S4)	Destabilized SL-SLBP complex. Destabilized ternary complex. Probably no effect on SL-3'hExo complex.
R181A	Recognizes the guanine base of the second nucleotide of the stem (Fig. 2A)	Destabilized SL-SLBP complex. Destabilized ternary complex. No apparent effect on SL-3'hExo complex.
H195A	π-stacking with the fourth base (C15) of the loop (Fig. 2B)	No apparent effect on SL-SLBP and ternary complexes.
3'hExo		
Y66A	Interacts with the second base (U13) of the loop (Fig. 2B)	Destabilized SL-3'hExo complex
A70E	Close contact with the second nucleotide of the loop (Fig. 2B)	Destabilized SL-3'hExo complex
R78A	Hydrogen bonds to the fourth base (C15) of the loop (Fig. 2B)	Destabilized SL-3'hExo complex
K104A	Interacts with the phosphate of A18 of the stem (Fig. S6)	No apparent effect on SL-3'hExo complex
K107A	Interacts with the phosphate of G17 of the stem (Fig. S6)	Destabilized SL-3'hExo complex

W233A	π-stacking with C25 of the 3' flanking sequence (Fig. 3A)	No apparent effect on SL-3'hExo complex
R261A	Interacts with the base and ribose of C24 and C25 (Fig. 3A)	Destabilized SL-3'hExo complex

1. Only a qualitative outcome of the experiment is given, using EMSA to assess the formation of the complex. While some mutations appear to have larger effects than others based on the gel, the actual impact on the affinity will require quantitative measurements.